

Optical Engineering

OpticalEngineering.SPIEDigitalLibrary.org

Metamaterial-based energy harvesting for GSM and satellite communication frequency bands

Mehmet Bakır
Muharrem Karaaslan
Faruk Karadağ
Emin Ünal
Oguzhan Akgöl
Fatih Ö. Alkurt
Cumali Sabah

Metamaterial-based energy harvesting for GSM and satellite communication frequency bands

Mehmet Bakır,^a Muharrem Karaaslan,^b Faruk Karadağ,^c Emin Ünal,^b Oguzhan Akgöl,^b Fatih Ö. Alkurt,^b and Cumali Sabah^{d,e,*}

^aBozok University, Department of Computer Engineering, Faculty of Engineering and Architecture, Yozgat, Turkey

^bIskenderun Technical University, Department of Electrical and Electronics Engineering, Iskenderun, Turkey

^cÇukurova University, Department of Physics, Adana, Turkey

^dMiddle East Technical University—Northern Cyprus Campus, Department of Electrical and Electronics Engineering, Kalkanli, Guzelyurt, TRNC/Mersin 10, Turkey

^eMiddle East Technical University—Northern Cyprus Campus, Kalkanli Technology Valley, Kalkanli, Guzelyurt, TRNC/Mersin 10, Turkey

Abstract. A metamaterial-based energy harvesting structure has been designed and experimentally tested in this study. The proposed structure has square and split ring resonators placed in different angles on the back and front sides for compatible multiband operation in energy harvesting. Resonance points have been defined at 900 MHz, 1.37 GHz, 1.61 GHz, 1.80 GHz, and 2.55 GHz, by simulation and experimental methods. These points correspond to Global System for Communication (GSM) 900, GSM 1800, Universal Mobile Telecommunication System (UMTS), satellite navigation, and Industrial Scientific and Medical (ISM) band frequencies. Supporting multiband application in a single structure without changing dimensions or design is one of the properties of this study. To harvest captured electromagnetic energy, an HSMS 2860 Schottky diode has been used. For wireless power transmission efficiency, voltage across the Schottky diode has been measured by a spectrum analyzer in different points experimentally. The maximum obtained voltage across the Schottky diode is 90 mV at 1800 MHz when a 500 mV signal is applied from a 5 cm distance. Simulated and experimental results prove that the proposed structure can effectively be used in GSM, satellite communication, and UMTS electromagnetic bands for energy harvesting and filtering applications. © 2018 Society of Photo-Optical Instrumentation Engineers (SPIE) [DOI: 10.1117/1.OE.57.8.087110]

Keywords: metamaterial; absorber; metamaterial energy harvesting; GSM bands.

Paper 180006 received Jan. 15, 2018; accepted for publication Aug. 8, 2018; published online Aug. 31, 2018.

1 Introduction

Metamaterials (MTMs) are artificial structures that exhibit exotic properties as negative refraction.¹ It is possible to absorb electromagnetic energy for different purposes within the MTMs.^{2–6} Radio frequency (RF) energy harvesting (EH) applications are generally based on metamaterial absorber (MA) that search widely⁷ by utilizing MTMs for sophisticated energy transfer. In contrast to the MA studies, which are developed for absorbing electromagnetic energy, EH studies are realized using a resistor or Schottky diodes for harvesting the energy collected on the gaps or splits on the resonators.^{8–10} Other types of EH applications are vibrational, thermal, and solar, which can be accomplished by electromechanical and/or thermoelectric systems.^{11–14} Microwave energy is such an ambient energy source due to substantial transmission of wireless communication systems. The idea of microwave EH depends on the energy that is normally lost on the environment. This energy can be used as a power source for small electronic devices.

In the first microwave EH study realized¹⁵ ~0.15 V harvested experimentally between 6 and 15 GHz. After that, an electrically small rectenna was designed and tested at the global positioning system (GPS) L1 frequency (1.5754 GHz).¹⁶ After using antenna in EH, a MTM EH study was initially reported by Ramahi et al.⁷ They designed a split ring resonator (SRR)-type MTM energy harvester that

operates at 5.8 GHz. A resistive load had been used as a lumped element to transfer RF energy to power. In 2013, Hawkes et al.¹⁷ designed and implemented a power harvesting MTM at the rate of 36.8% at 900 MHz. The signal was experimentally rectified by a Greinacher circuit, which is placed in the SRR that has two Schottky diodes connected parallel to double the output voltage with the efficiency of 36.8%. In 2014, Alavikia et al.¹⁸ introduced a class of electrically small resonators composed of complementary SRR backed by a ground plane that is used for EH at 5.8 GHz. Microwave energy is transferred using a resistive load again. Again in 2014, Almoneef and Ramahi proposed three-dimensional MTM stacked arrays for efficient conversion of electromagnetic energy into AC.¹⁹ In that proposal, several vertically stacked arrays in which each array is comprised of multiple SRR elements and resistive loads connected across the gaps takes place for EH at 5.8 GHz. In 2015, Alavikia et al.²⁰ demonstrated a ground backed complementary split ring resonator (G-CSRR) study with a power conversion efficiency of 92%. Another study in 2015 proposed by Almoneef and Ramahi²¹ is related to the increase of efficiency in the earlier work. That work emphasized the importance of SRR arrays in the usage of EH. In 2016, Duan et al.²² presented a planar MTM harvester to convert incident electromagnetic wave to direct current with rectifying functionality. It consisted of 6 × 6 MTM particles integrated with miniaturized rectifiers showing 44.5% efficiency at 2.45 GHz. In 2017, Tékam

*Address all correspondence to: Cumali Sabah, E-mail: sabah@metu.edu.tr

et al.²³ presented a microwave energy harvester based on a cutwire metasurface with an integrated PN junction diode at 6.75 GHz. New studies regarding EH in 5G networks were studied by Liu et al.²⁴

This study differs from other studies in some aspects with advantages and disadvantages. The first important part of this study is that the proposed design is especially configured to work in GSM 900, GSM 1800, and ISM bands, which mean 900, 1800, and 2550 MHz without changing the design. When we look at the similar studies in Refs. 25–27, it is necessary to change the design or adjust the air gap behind the MTM to harvest energy in GSM 900, GSM 1800, and ISM bands. In contrast to these studies, the proposed structure covers three bands without making any changes due to its special design. Air gap thickness is set to 5.6 mm according to parametric study results of the CST Microwave Studio (MWS) program.

Antenna-based wireless power transfer studies have been widely used by different scientists for EH.^{28–31} Another difference of this study is related to its design: it is MTM based. MTMs have widely been used in near to infrared absorber studies. This study demonstrates the MTM-based EH applications for GSM and ISM bands. By adding voltage double circuits, and using outdoor RF sources as GSM base stations, the proposed structure could be more productive since their RF power ranges from 40 to 100 W. Due to limitations in our laboratory, we used a 20-mW RF source for the experimental validation.

As will be shown in this paper, return loss at that frequency is low as wished for maximum EH ratio. In addition, one of the important aspects of this study is that the proposed structure is designed as an SRR-based chiral MTM to be novel in this area. The other advantage of this study is that it shows tunable property using air gap or lumped element with a resistor. By changing the air gap, it is possible to tune the resonance frequency of the EH system or it is possible to change the Schottky diode with the resistor to change the resonance frequency of the proposed design. As briefly explained here, most wireless devices operate within the operation frequency band of the proposed system; using a single structure, it is possible to harvest energy between 900 and 2550 MHz. Another important point in this study is the wireless power transfer ratio; wireless power transfer efficiency of the design is measured by a signal generator and spectrum analyzer between 5 and 75 cm. Findings are

reported in a table together with efficiency values. The organization of this study is as follows. In Sec. 2, the structure geometry based on chiral SRR is proposed, and the numerical method is presented. In Sec. 3, numerical and experimental results are presented and compared. Finally, a summary and conclusions are provided and discussed in Sec. 4.

2 Design and Numerical Setup

In this study, MTM is composed of SRRs proposed for GSM band EH. The proposed structure-based resonators are placed on a FR4 substrate, the FR4 substrate has a thickness of 1.6 mm and dielectric constant of 4.2, and the resonators are made up of copper that has a thickness of 0.035 mm and conductivity of 5.8×10^8 S/m. The lumped element that is used for harvesting microwave energy is a Schottky diode of HSMS 2860. As shown in Figs. 1(a)–1(c), the front side and back side resonators are not placed symmetrically. There is an air gap between the copper plate and back side resonators. This air gap is used for shifting the resonance frequency. As the structure contains a metallic back resonator, it is possible to tune the resonance frequency of the proposed structure by adjusting the placement of the front and back resonators as well as their dimensions. Front and back resonator do not have an electrical connection since they are used for manipulating the electromagnetic energy. As the structure contains a metallic back plate with a thickness of more than skin depth, the transmission value for the structure is zero. Hence, the absorption entirely depends on the reflection from the structure and absorption can be maximized by minimization of reflection. The most important part of the structure is design and placement of the front and back side resonators. Resonator dimensions are adjusted according to parametric study results run on a CST MWS. As will be seen in the simulation and test results, the proposed structure's reflection coefficient value (S_{11}) is minimum at the GSM resonance frequencies of 900, 1800, and 2550 MHz. When we look at the resonators in the front and back sides of the FR4 substrate, square SRR is placed outside the structure and has a length of 34 mm, and SRR that is placed inside the proposed structure has a diameter of 34 mm. The width of split is adjusted to 2 mm for both of them. SRR that is placed on the inner side of the resonator in the front and back sides have been placed differently with an angle of 45 deg and 125 deg. These angles are adjusted according to maximum efficiency in EH for GSM bands. The air gap that is placed

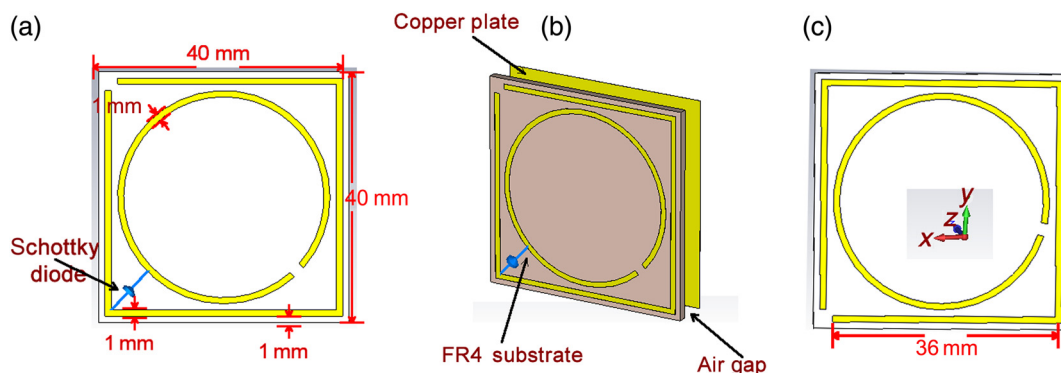


Fig. 1 Proposed structure for GSM band EH (a) front side, (b) profile view of the proposed structure, and (c) back view of the proposed structure.

between back resonator and copper plate is set to 5.6 mm for maximum EH efficiency.

Numerical simulation results are obtained by a CST MWS that is commercially available and utilizes finite integration technique. Absorption can be defined as no transmission and reflection in the case of an incident radiation. Absorption can be determined as $A(\omega) = 1 - R(\omega) - T(\omega)$, where $A(\omega)$, $R(\omega)$, and $T(\omega)$ define the absorption, reflectance, and transmittance, respectively. When reflection $R(\omega) = |S_{11}|^2$ and transmission $T(\omega) = |S_{21}|^2$ fall to the minimum values, absorption rises to the maximum level at the resonance frequency. There will be no transmission to be examined since a metal plate is placed behind the air gap. To harvest microwave energy, it is necessary to absorb it in the MTM. For this reason, harvested energy rises when perfect absorption occurs. This energy can be harvested using a high frequency Schottky diode. In this study, a HSMS 2860 Schottky diode is used both in the simulation and experimental study parts. It is possible to reduce reflection to almost zero by choosing the relative effective permittivity $\epsilon(\omega)$ and permeability $\mu(\omega)$ values carefully to provide impedance matching with the air. It is possible to absorb both the incident electric and magnetic field by properly tuning $\epsilon(\omega)$ and $\mu(\omega)$ of the effective medium of the absorber.

3 Results and Discussion

To show the performance of the proposed structure, it is necessary to analyze the reflection coefficient in dB. For this reason, it is numerically analyzed and experimentally verified. Also, the Schottky diode used in this study to harvest microwave energy is placed between the outside and inner side resonators as shown in Fig. 1. Since Schottky diodes have unique characteristics, they will affect the resonance frequencies because of the matching impedance where they have been used. For this reason, a single Schottky diode has been used and no other lumped element is used in this study for perfect absorption at the GSM band frequencies. Schottky diodes used in this study have no serial or parallel connection as designed. This is an advantage since effects of the circuit parameters have been ignored. First of all, to show the S_{11} reflection coefficient of the proposed structure, it is produced using a CNC controlled PCB production machine; after that, the S_{11} parameter is measured using a two horn antenna and vector network analyzer, as shown in Fig. 2. Two horn antennas have been used to

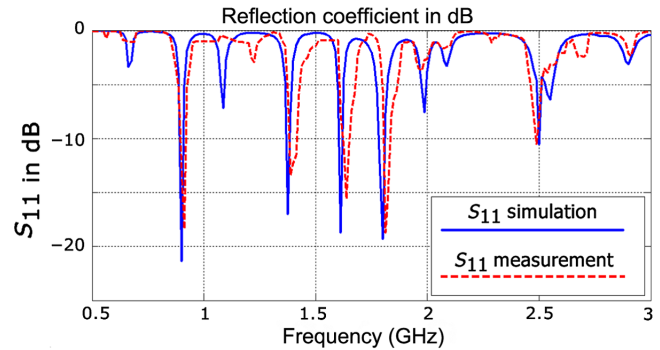


Fig. 3 Simulated and measured reflection coefficient (magnitude in dB) of the proposed structure under unit cell boundary conditions between 500 MHz and 3 GHz.

see the transmission coefficient since that parameter is affecting the absorption value according to equation $A(\omega) = 1 - R(\omega) - T(\omega)$. When it is measured, its value is very small due to the copper plate behind the air gap; for this reason, $T(\omega)$ is assumed to be zero.

Simulated and measured reflection coefficient graphs are given in Fig. 3. Small differences between them occurred due to calibration and test errors in the laboratory. As shown in Fig. 3, resonance frequencies are determined as 900 MHz, 1.37 GHz, 1.61 GHz, 1.80 GHz, and 2.55 GHz, respectively, between 500 MHz and 3 GHz. Because the proposed design is an instance of MTM absorber, resonance points significantly increased. As shown in Fig. 3, S_{11} parameters are apparently high and generally agree at resonance points as expected. One of the aims of the study is to have a simple structure that can easily be produced and have some resonances at GSM and satellite communication bands, which is proposed by the suggested design.

To explain the absorption mechanism of the proposed structure, the surface current distribution and electric energy densities are studied at the resonance frequency of 900 MHz, which is the resonance frequency defined both experimentally and numerically. The simulated surface current distribution is given in Fig. 4(a); the figure shows that the electric energy is concentrated at the left bottom side of the resonators. The structure provides an independent electric response at the resonance, as in the pattern of the electrical dipole. As a result, the surface charge oscillates along the external electric field. This electric response excites free

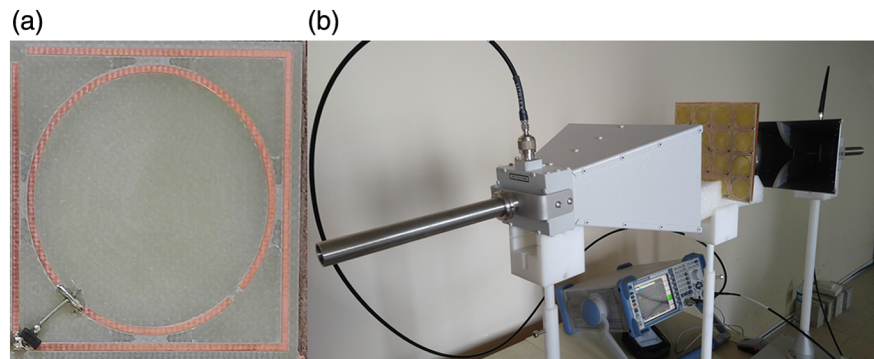


Fig. 2 (a) Closer look at the manufactured sample and (b) picture from a test for measuring scattering parameters.

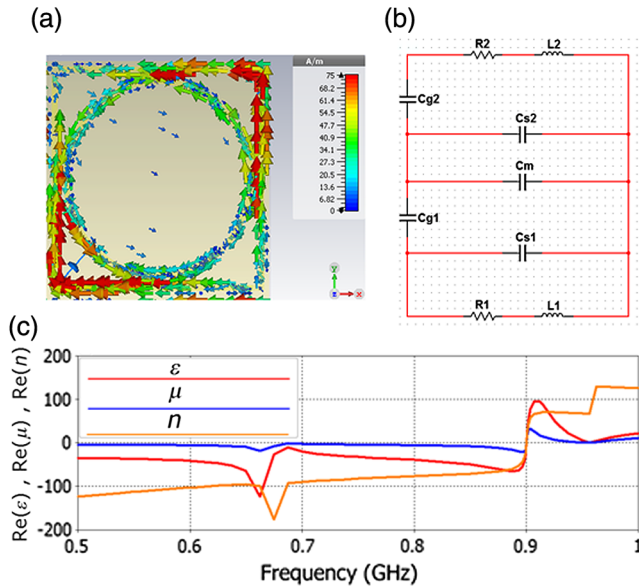


Fig. 4 (a) Simulated surface current distribution, which is showing parallel and antiparallel currents at 900 MHz, (b) equivalent circuit model of the proposed EH structure, and (c) real part of dielectric permittivity, permeability, and refractive index between 500 MHz and 1 GHz.

electrons as a surface current. For this reason, the magnetic dipole moment due to the surface current charges induces a magnetic response. This magnetic response, consequently, causes a resonant absorption. Moreover, there are parallel and antiparallel surface currents on the structure. Parallel currents induce an electric field, whereas the antiparallel currents induce a magnetic field. These responses couple with E and H components of the incident EM wave and produce a strong localized EM field at the resonance frequency. As shown in Fig. 4(a), there is surface current distribution difference between inner and outer resonators that is strong at the outer resonator due to the incident electromagnetic wave. This difference causes a voltage difference between the inner and outer resonator, which can be read from the poles of the Schottky diode at the resonance frequencies as shown in the EH section.

To explain resonance characteristics of the proposed structure, Fig. 4(b) is plotted. $R1$ and $R2$ indicate total power loss of the proposed EH structure in the resonator parts. The overall inductance $L1$ and $L2$ consist of the unit cell resonator with mutual inductance. $Cs1$ and $Cs2$ originate from the mutual capacitance between neighboring unit cells. $Cg1$ and $Cg2$ are the effects of capacitive gaps placed in the front and back resonators, which provide charge by the external field. Finally, Cm is the mutual capacitance between the front and back side resonators.^{32–33} As briefly shown here, resonance frequencies and resonance peaks depend on both resonator shapes and the air gap, which is placed between back resonator and copper back.

After explaining surface current distribution and equivalent circuit model of the proposed EH structure, effective circuit parameters obtained between 500 MHz and 1 GHz are shown in Fig. 4(c). Dielectric permittivity, permeability, and refractive index of the proposed structure are negative between 500 and 900 MHz. At 900 MHz, a sudden change occurs due to sudden resonance peaks.

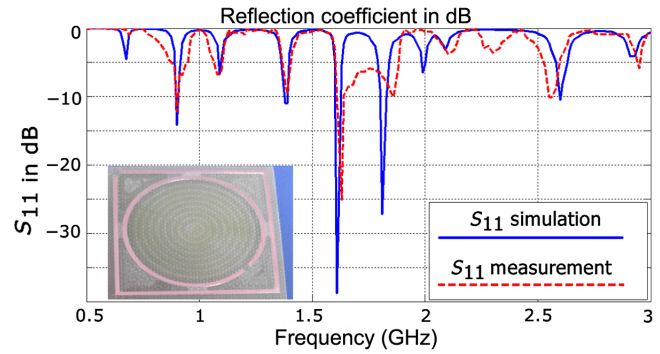


Fig. 5 Simulated and measured absorption values of the proposed structure Schottky diode not used as a lumped network element.

3.1 Effects of Schottky Diode

To show the effects of using a Schottky diode, the Schottky diode is removed from the proposed structure, and the simulation together with the experimental study to define the absorption value is studied. As shown in Fig. 5, absorption resonance frequencies have not significantly changed. Resonance at 1800 and 2550 MHz shifted to 1810 and 2600 MHz, respectively. Test results also verify the simulation results with some differences caused by calibration and test results. When absorption results are compared with each other, the Schottky diode effect can be accepted as negligible. When we look at the experimental results, they generally comply with the simulation results. Simulated S_{11} in the dB level is considerably higher than the experimental results, and there is a resonance shift between them because of the calibration and manufacturing errors together with the testing environment.

Instead of a Schottky diode, a resistor can be used to harvest energy as a load resistor. To show the effects of the resistor value on harvested energy, a set of simulations is prepared. In this case, a resistor value is changed between 5 and 50 Ω with a step of 5 Ω . Simulation results show the RF to DC conversion performance. As is generally known, the RF to DC conversion value is important for the efficient EH design, which will be calculated as Ref. 7 ,

$$\rho = \frac{P_{DC}}{P_{RF}}, \quad (1)$$

where P_{RF} is defined as 0.5 W by the simulation program manufacturer. These simulation power data have been taken from the simulation program by choosing the monitor voltage and current section in the lumped network element. Simulated power data are taken from the accepted power section at the simulation results. P_{DC} values are extracted from the voltage and current values of the resistors used in this study. For numerical validation, resistors are placed between outside and inside resonators instead of Schottky diodes. In this case, the power harvesting efficiency graph is given in Fig. 6, at 900 MHz. As seen from the figure, simulated power on different resistance values decreases as the resistance value increases. Maximum power efficiency is found numerically; it is 0.40 W between 5 Ω and 10 Ω and decreases linearly between 10 Ω and 50 Ω . Minimum power harvesting efficiency is 0.18 W.

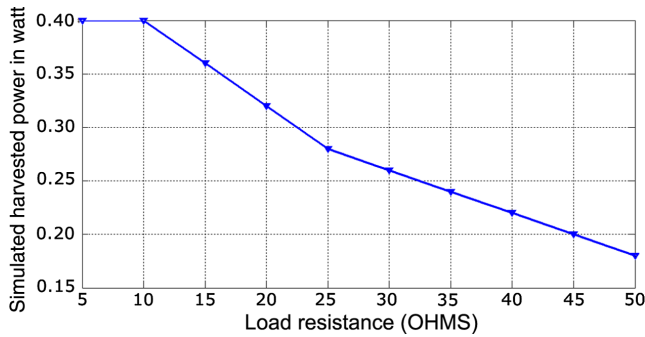


Fig. 6 Simulated harvested power in watt according to different resistor values that is used as a lumped network element.

3.2 Effects of Air Gap on Reflection Coefficient

A copper plate is placed 4 mm away from the back side resonators to increase the absorption rate directly, which affects the harvested power efficiency and resonance frequency of the proposed EH system. In this part, two numerical simulations are prepared; the first one is the air gap distance and absorption relation, and the second one is related to the removal of the copper plate. In this case, we have removed the copper plate, harvested energy is simulated, and the numerical and experimental reflection coefficient is presented.

For the purpose of assessment, first, the copper plate is not removed and the air gap thickness is adjusted between 1.6 and 5.6 mm with a step of 2 mm. The $[S_{11}]$ in the dB spectra were simulated using CST MWS. Furthermore, simulated power between the Schottky diode was simulated at 900 MHz; results are presented in Table 1. As shown in Fig. 7, the air gap between the backside resonator and copper plates has a shifting effect on the reflection coefficient, and signal magnitude level maximum absorption occurs at the 5.6-mm air gap distance. Also, at this distance, the GSM 900, GSM 1800, and UMTS bands are covered, and there are four different resonance points at 900 MHz,

Table 1 Energy harvesting efficiency comparison table (single array).

Simulated power at 900 MHz	Efficiency
Airgap = 1.6 mm	30% (0.30 W)
Airgap = 3.6 mm	38% (0.38 W)
Airgap = 5.6 mm	40% (0.40 W)

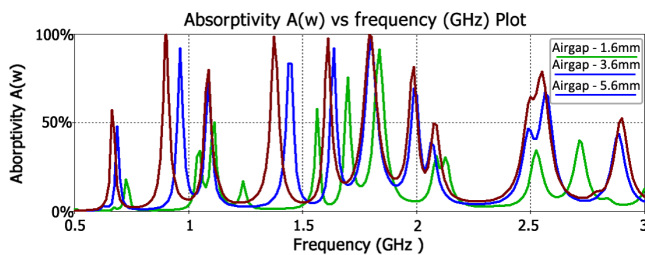


Fig. 7 Reflection coefficient in dB according three different air gap values.

1.37 GHz, 1.61 GHz, and 1.8 GHz. As the distance decreases, the resonance frequency shifts upward due to the capacitive effects of the plate. As is generally known, the parallel plate capacitors’ capacitance value depends on the distance of parallel plates and the surface area of the plates. When we look at Fig. 7, the resonance frequency shifts downward between 0.5 and 3 GHz due to the effects of parallel plates.

3.3 Effects of Polarization Angle and Incident Angle

In this section, the theta and phi polarization angle with incident angle dependency is simulated using CST MWS. To realize these simulations, the proposed MTM, which is presented as in Fig. 1, is prepared; after that, the simulation setup is completed according to simulation program settings. After finishing these preadjustments, reflection coefficient according to the phi angle is simulated; obtained results are presented in Figs. 8 and 9. As shown in these figures, the reflection coefficient is not affected by the phi and theta polarization angles, which is good for harvesting efficiency. Another simulation presented here is the incident angle dependency of the proposed structure. To realize this, two different incident angle values, which are 0 deg and 30 deg, have been taken as samples; the simulated incident angle dependency is shown in Fig. 10.

As shown in Fig. 10, when the incident angle changes, it affects the reflection coefficient by both resonance shifts and the dB level. This is related to the design details of the proposed structure as the place of the Schottky diode and resonators.

3.4 Energy Harvesting and Wireless Power Transfer

In this section, EH and wireless power transfer performance of the proposed structure have been determined. First, simulated power harvesting efficiency is presented using CST MWS between 500 MHz and 3 GHz. As shown in Fig. 11, harvested power at the resonance points, which

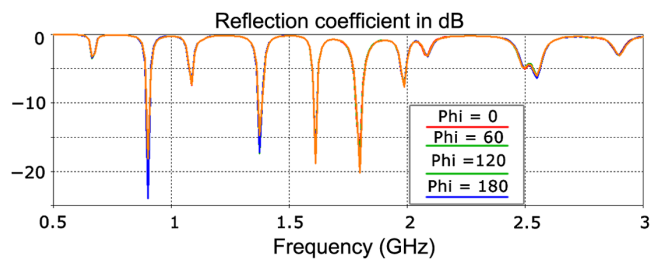


Fig. 8 Effects of phi angle in reflection coefficient.

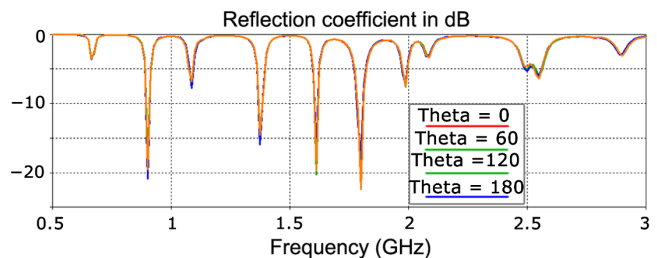


Fig. 9 Effects of theta angle in unit cell boundary.

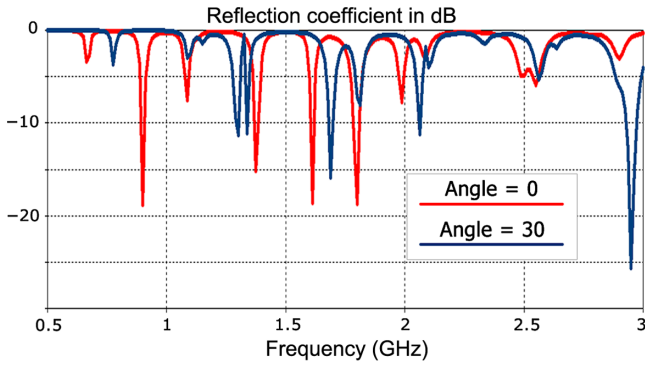


Fig. 10 Effects of incident angle on reflection coefficient.

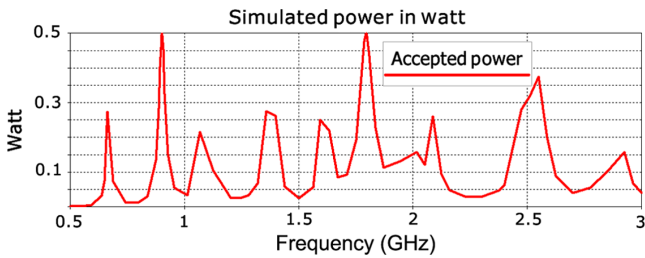


Fig. 11 (a) Simulated power in watt between 500 MHz and 3 GHz.

are at 900 MHz, 1.37 GHz, 1.61 GHz, 1.80 GHz, and 2.55 GHz, are changing between 0.2 and 0.5 W. Especially at 900 and 1800 MHz, a 0.5-W value is remarkable since the simulation program produces 0.5-W power during simulation, which means that energy is fully absorbed and unity efficiency has been obtained at the resonance frequencies of GSM bands. To support simulation results, we have realized a spectrum analyzer measurement across

an HSMS 2860 Schottky diode, which will be explained in this section. The bandwidth of the EH intervals at resonance frequencies is small. However, this is a disadvantage; when we think about the bandwidth of GSM and ISM bands, this study has compatible use in these bands. To compare the simulated power harvesting efficiency with similar studies, Table 2 is prepared. While EH efficiency starts from smaller values as 47%, it reaches up to 100% due to advances in this field. The proposed structure also has 100% simulated power harvesting efficiency.

According to simulated power in watt, the proposed structure covers more than three bands. However, due to maximum power efficiency, only three bands were chosen for samples. In the same table, we also compare the measured results with similar studies. As seen clearly, RF to DC conversion is smaller since this study is not rectenna based. The other studies are using a rectifier with antenna and cascade connected RF diodes to increase power efficiency.

To show the spectrum analyzer view between 500 MHz and 3 GHz, we connected the spectrum analyzer using a cable across the HSMS 2860 Schottky diode as shown in Fig. 12. As shown in the figure, the proposed structure was produced in a 2 × 2 unit cell, and only one of the Schottky diodes on the structure is connected to a spectrum analyzer. The reason for this setup is to create a periodic boundary effect as in the other sections of the study. The horn antenna is Schwarzbeck BBHA 9120, which has a compatible operation between 800 and 5200 MHz RF. The horn antenna is connected to a network analyzer that is operating in S_{11} measurement mode. After completion of this measurement setup, we obtained a spectrum analyzer view, which is given in Fig. 13.

According to Figs. 3 and 13, Table 3 is prepared to give brief information about the S_{11} reflection coefficient and signal increment at the resonance points. Both resonance points are generally compatible with each other. However, due to

Table 2 Comparison table of measured and simulated power efficiency with other studies.

Power efficiency comparison table	This study	Almoneef and Ramahi ⁸	Alavikia et al. ¹⁸	Bakir et al. ¹⁰	Alavikia et al. ²⁰	Gabin et al. ⁹	Almoneef et al. ³²
Simulated (%)	100	47	84	87	92	100	100
Measured (%)	39	Not available	60	Not available	60	50	80

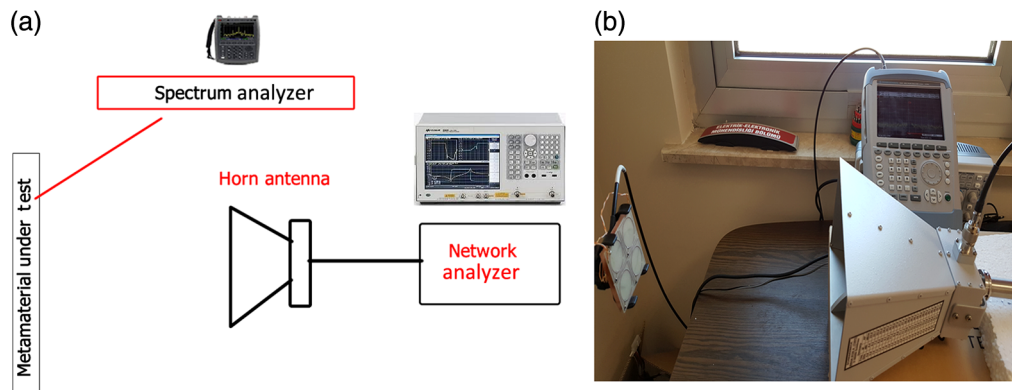


Fig. 12 (a) Test schematic for spectrum analyzer measurements and (b) real picture of the experiment.

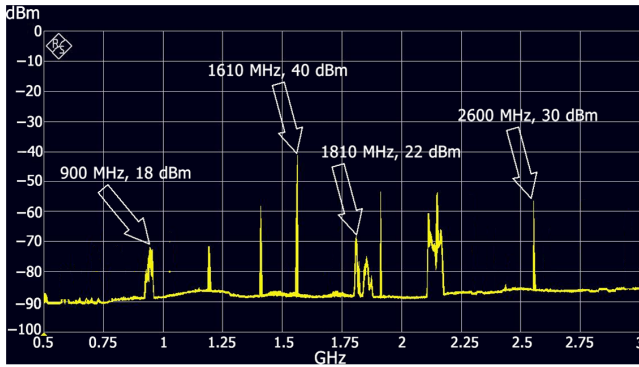


Fig. 13 Spectrum analyzer view of the proposed structure across the HSMS 2860 Schottky diode between 500 and 3000 MHz when network analyzer is operated between these frequencies.

external effects and calibration errors, signal levels are not compatible with each other as in 2.55 GHz. Another point that affects this value is the antenna gain values at different frequencies. Antenna gains have different values at different frequencies, which are indicated by the manufacturer of the horn antenna on the device. Figure 13 is taken directly from the spectrum analyzer output file, which shows the signal level increase around the resonance points of the proposed structure. It is very clear from the figure that maximum signal level is observed around 1600 and 1900 MHz, which complies with the maximum reflection coefficient level and their resonance points. The maximum signal increase is 45 dBm at 1600 MHz; there are also different signal increments present at difference resonance points as expected, which can be seen in Fig. 13. While 20 and 30 dBm differences are seen at 900 and 1800 MHz, respectively, during spectrum analyzer measurement, reflection coefficient measurement values are presented. According to Table 3, test measurements generally comply with each other.

For comparison of measured spectrum analyzer results in Fig. 13 with simulated power in Fig. 11, Table 4 is prepared. As seen, some of the resonance points cannot be seen during spectrum analyzer measurement. These errors are caused by the calibration and testing environment. Since these points



Fig. 14 Experimental test setup for wireless power transfer.

are not used for EH in this study, the effects of these points on overall structure are minimal.

To show the wireless power transfer performance, another experimental validation was made. In this validation, a vector network analyzer was taken and the TTR2050 signal generator was connected to the horn antenna while the spectrum analyzer is still connected to the Schottky diode on the unit cell, which is shown in Fig. 14.

According to the measurement setup that is given in Fig. 14, the signal generator output is set to 500 mV and is connected to the spectrum analyzer to see the cable and other losses. The spectrum analyzer shows 497 mV with a power of 2 mW input value at 1610 MHz as shown in Figs. 15(a) and 15(b). According to this input, we have not seen any loss that affects the horn antenna input due to cable and signal generator. When we connect the signal generator to the horn antenna and measure the signal level on the Schottky diode, which is connected to the spectrum analyzer, the following distance versus voltage level across the Schottky diode table is prepared. As shown in Table 5, distance and voltage level are indirectly proportional to each other, which means that as the distance increases, measured voltage as well as power across the diode decreases in accordance with the Friis equation given below since output power is inversely proportional to distance. This value can be increased using different rectenna circuits

Table 3 S_{11} reflection coefficient and spectrum analyzer measurement result comparison table.

Resonance type	Resonance frequency in GHz. and signal level in dB for network analyzer spectrum analyzer in dBm (increment)						
S_{11}	0.9/ - 18 dB	1.08/ - 7 dB	1.370/ - 15 dB	1.61/ - 15 dB	1.8/ - 18 dB	2/ - 7 dB	2.55/ - 6 dB
Spectrum analyzer	0.9/18 dBm	1.2/18 dBm	1.38/30 dBm	1.61/18 dBm	1.8/22 dBm	2.1/20 dBm	2.6/30 dBm

Table 4 Resonance frequency comparison table of measured spectrum analyser results with simulated power in Fig. 11.

Simulation / experimental	Resonance frequencies								
Simulated power	660 MHz	900 MHz	1.06 GHz	1.37 GHz	1.61 GHz	1.8 GHz	2.08 GHz	2.55 GHz	2.92 GHz
Spectrum analyzer	None	900 MHz	1.2 GHz	1.38 GHz	1.61 GHz	1.8 GHz	2.1 GHz	2.6 GHz	None

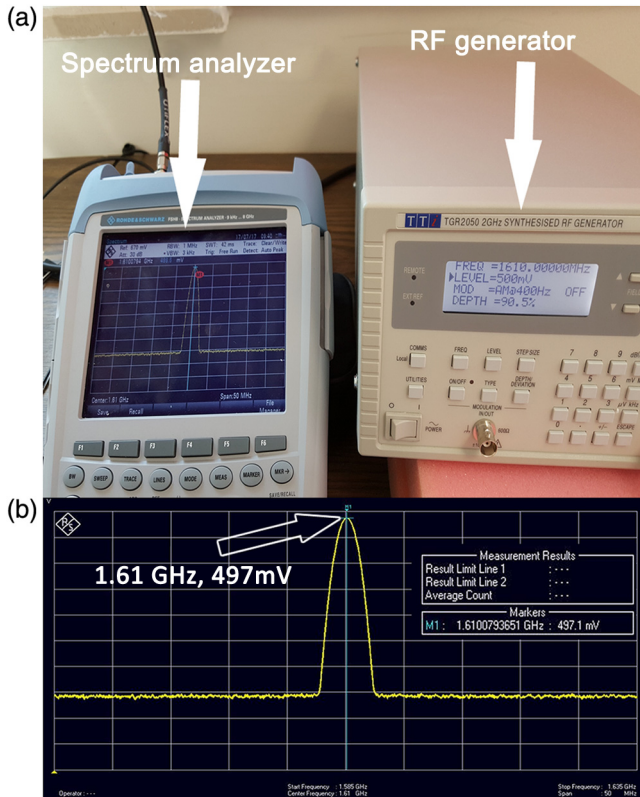


Fig. 15 (a) Signal generator output at 1610 MHz, and spectrum analyzer view of the applied signal, which is emphasized by marker at 1610 MHz and (b) spectrum analyzer direct view of the signal generator output defined as 497 mV at 1610 MHz.

$$\frac{P_r}{P_t} = G_t G_r \left(\frac{\lambda}{4\pi R} \right)^2 \quad (2)$$

As shown in Fig. 16, marker position is set to 1.61 GHz and voltage level across the HSMS 2860 Schottky diode, which is measured by spectrum analyzer, is 81 mV at 5 cm, 36 mV at 20 cm, and 1.8 mV at 75 cm. When the input value has been accepted as 497 mV, efficiency of the EH system at 5 cm is P_{out}/P_{in} , meaning $81/497 = 16\%$; this value decreases to 7% at 20 cm and 0.4% at 75 cm. Although, these values are small when compared with wireless power transfer studies realized in MHz frequency level,^{34–36} they can be used as a reference in GHz frequency band.

Table 5 Spectrum analyzer readings according to horn antenna and proposed structure distances set to 5, 10, 20, 35, 50, and 75 cm when 2-mW power is applied.

Measured voltage and DC power efficiency at	0.05 m	0.1 m	0.2 m	0.35 m	0.5 m	0.75 m
1610 MHz/voltage	81 mV	46 mV	36 mV	20 mV	11 mV	1.8 mV
1610 MHz/power efficiency	31%	10%	6%	1.95%	0.6%	0.1%
1800 MHz	90 mV	44 mV	34 mV	17 mV	12 mV	7 mV
1610 MHz/power efficiency	39%	9.9%	5.7%	1.72%	0.61%	0.25%

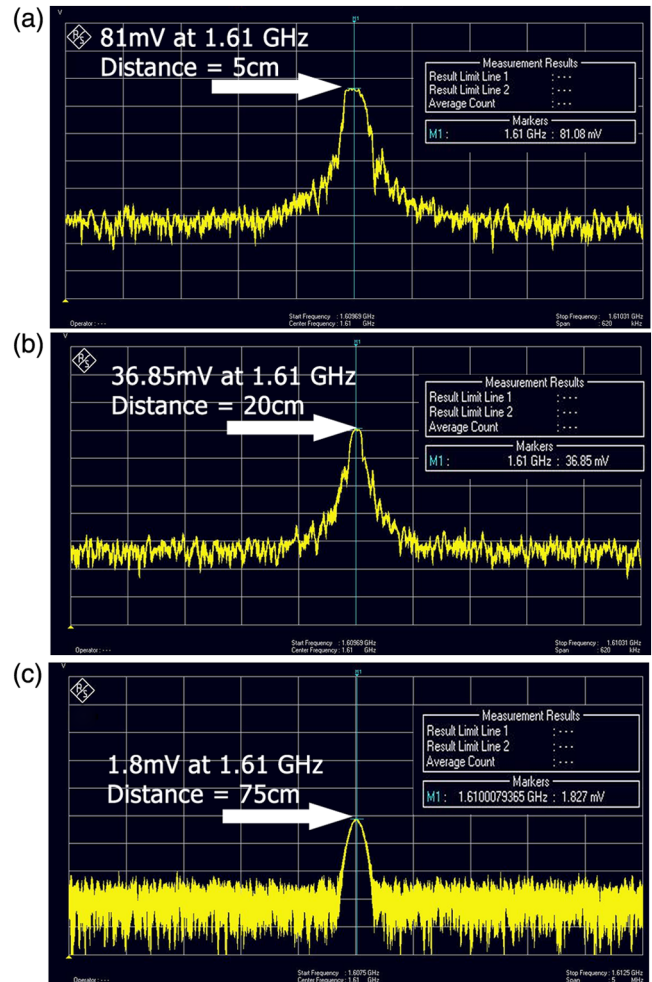


Fig. 16 (a) Schottky diode spectrum analyzer view when the wireless power transfer horn antenna is placed at different distances and spectrum analyzer marker is set to 1.61 GHz. (a) 5 cm and 81 mV output, (b) 20 cm and 36 mV, and (c) 75 cm and 2 mV values have been read.

4 Conclusion

In this study, a MTM-based EH structure is proposed. This structure design dimensions are adjusted to operate between 500 MHz and 3 GHz, especially for GSM band frequencies. A set of simulations that are verified by experimental measurements covering S_{11} parameter and spectrum analyzer measurements for EH and wireless power transfer have been supplied. The design dimensions are especially chosen for EH at GSM 900 MHz, 1800 MHz, satellite

communication, and UMTS frequency bands, which are the most common frequency bands for mobile devices. This study has unique characteristics of three bands being covered in a single design when it is compared with other EH studies. This point is very important for mobility and easiness of usage since no dimension adjustment is necessary as in Ref. 17. Simulated and measured resonance frequencies in S_{11} measurement have been defined as 900 MHz, 1.37 GHz, 1.61 GHz, 1.80 GHz, and 2.55 GHz, respectively, between 500 MHz and 3 GHz. A comprehensive study that covers network analyzer measurements, spectrum analyzer measurements, and voltage measurements has been realized. At 1.6 GHz, the signal increased from -90 to -40 dBm, which is in about 50 dBm increments. Also, wireless power transfer measurements were realized using a spectrum analyzer and signal generator. Wireless power transfer performance was measured from six different points from 5 to 75 cm. Wireless power transfer efficiency was measured to be 17% at 5 cm. Simulation and experimental study results generally comply with each other; small differences occur due to calibration and test environment as well as effects or harmonics coming from outside. This study will be used as a reference in GSM band EH studies. For future work, power transfer efficiency can be increased using a different design and using powerful resources as base station transmitters since their power ranges from 40 to 100 W. Using these types of powerful RF sources will increase the distance away from 75 cm and harvested power quantity.

References

- R. A. Shelby, D. R. Smith, and S. Schultz, "Experimental verification of a negative index of refraction," *Science* **292**(5514), 77–79 (2001).
- C. Sabah et al., "Perfect metamaterial absorber with polarization and incident angle independencies based on ring and cross-wire resonators for shielding and a sensor application," *Opt. Commun.* **322**, 137–142 (2014).
- F. Dincer et al., "Polarization angle independent perfect metamaterial absorbers for solar cell applications in the microwave, infrared, and visible regime," *Prog. Electromagn. Res.* **144**, 93–101 (2014).
- B. Wang, T. Koschny, and C. M. Soukoulis, "Wide-angle and polarization-independent chiral metamaterial absorber," *Phys. Rev. B* **80**, 033108 (2009).
- F. Ding et al., "Ultra-broadband microwave metamaterial absorber," *Appl. Phys. Lett.* **100**, 103506 (2012).
- H. Wang et al., "Broadband tunability of polarization-insensitive absorber based on frequency selective surface," *Sci. Rep.* **6**, 23081 (2016).
- O. M. Ramahi et al., "Metamaterial particles for electromagnetic energy harvesting," *Appl. Phys. Lett.* **101**, 173903 (2012).
- T. S. Almoneef and O. M. Ramahi, "A 3-dimensional stacked metamaterial arrays for electromagnetic energy harvesting," *Prog. Electromagn. Res.* **146**, 109–115 (2014).
- T. Gabin et al., "Designing an efficient rectifying cut-wire metasurface for electromagnetic energy harvesting," *Appl. Phys. Lett.* **110**(8), 083901 (2017).
- M. Bakir et al., "Electromagnetic energy harvesting and density sensor application based on perfect metamaterial absorber," *Int. J. Mod. Phys. B* **30**(20), 1650133 (2016).
- Q. Li, Y. Kuang, and M. Zhu, "Auxetic piezoelectric energy harvesters for increased electric power output," *AIP Adv.* **7**(1), 015104 (2017).
- L. Xiong, L. Tang, and B. R. Mace, "Internal resonance with commensurability induced by an auxiliary oscillator for broadband energy harvesting," *Appl. Phys. Lett.* **108**, 203901 (2016).
- W. Deng and Y. Wang, "Systematic parameter study of a nonlinear electromagnetic energy harvester with matched magnetic orientation: numerical simulation and experimental investigation," *Mech. Syst. Sig. Process.* **85**, 591–600 (2017).
- H. Jopek, "Finite element analysis of tunable composite tubes reinforced with auxetic structures," *Materials* **10**(12), 1359 (2017).
- J. A. Hagerly and Z. B. Popovic, "An experimental and theoretical characterization of a broadband arbitrarily polarized rectenna array," in *IEEE MTT-S Int. Microwave Symp. Digest*, Vol. 3, pp. 1855–1858 (2001).
- N. Zhu, R. W. Ziolkowski, and H. Xin, "A metamaterial-inspired, electrically small rectenna for high-efficiency, low power harvesting and scavenging at the global positioning system L1 frequency," *Appl. Phys. Lett.* **99**, 114101 (2011).
- A. M. Hawkes, A. R. Katko, and S. A. Cummer, "A microwave metamaterial with integrated power harvesting functionality," *Appl. Phys. Lett.* **103**, 163901 (2013).
- B. Alavikia, T. S. Almoneef, and O. M. Ramahi, "Electromagnetic energy harvesting using complementary split-ring resonators," *Appl. Phys. Lett.* **104**, 163903 (2014).
- T. Almoneef and O. M. Ramahi, "Metamaterial electromagnetic energy harvester with near unity efficiency," *Appl. Phys. Lett.* **106**, 153902 (2015).
- B. Alavikia, T. S. Almoneef, and O. M. Ramahi, "Complementary split ring resonator arrays for electromagnetic energy harvesting," *Appl. Phys. Lett.* **107**, 033902 (2015).
- T. Almoneef and O. M. Ramahi, "Split-ring resonator arrays for electromagnetic energy harvesting," *Prog. Electromagn. Res. B* **62**, 167–180 (2015).
- X. Duan, X. Chen, and L. Zhou, "A metamaterial harvester with integrated rectifying functionality," in *Int. Conf. on Wireless Information Technology and Systems (ICWITS) and Applied Computational Electromagnetics (ACES)*, Honolulu, Hawaii, pp. 1–2 (2016).
- G. T. Tekam et al., "Designing an efficient rectifying cut-wire metasurface for electromagnetic energy harvesting," *Appl. Phys. Lett.* **110**, 083901 (2017).
- Y. Liu et al., "Integrated energy and spectrum harvesting for 5G wireless communications," *IEEE Network* **29**(3), 75–81 (2015).
- M. Piñuela, P. D. Mitcheson, and S. Lucyszyn, "Ambient RF energy harvesting in urban and semi-urban environments," *IEEE Trans. Microwave Theory Tech.* **61**(7), 2715–2726 (2013).
- L. Yang et al., "Compact multi-band wireless energy harvesting based battery-free body area networks sensor for mobile healthcare," *IEEE J. Electromagn. RF Microwaves Med. Biol.* **2**(2), 109–115 (2018).
- M. Bakir et al., "Tunable energy harvesting on UHF bands especially for GSM frequencies," *Int. J. Microwave Wireless Technol.* **10**, 1–10 (2017).
- M. Dini et al., "A fully-autonomous integrated RF energy harvesting system for wearable applications," in *European Microwave Conf.*, pp. 987–990 (2013).
- U. S. Pranav et al., "Metamaterial based energy harvester," *Procedia Comput. Sci.* **93**, 74–80 (2016).
- M. Mrnka et al., "The RF energy harvesting antennas operating in commercially deployed frequency bands: a comparative study," *Int. J. Antennas Propag.* **2016**, 1–11 (2016).
- K. A. Devi et al., "Investigations on characteristics of metamaterial based patch antenna for RF energy harvesting at GSM 900," *Electr. Electron. Eng.* **5**(1A), 7–13 (2015).
- T. Almoneef, F. Erkmén, and O. M. Ramahi, "Harvesting the energy of multi-polarized electromagnetic waves," *Sci. Rep.* **7**, 14656 (2017).
- A. Sellier, T. V. Teperik, and A. Lustrac, "Resonant circuit model for efficient metamaterial absorber," *Opt. Express* **21**(106), A997–A1006 (2013).
- B. Bhattacharyya, G. Saptarshi, and K. V. Srivastava, "Equivalent circuit model of an ultra-thin polarization-independent triple band metamaterial absorber," *AIP Adv.* **4**(9), 097127 (2014).
- B. Wang et al., "Wireless power transfer with metamaterials," in *Proc. of the 5th European Conf. on Antennas and Propagation (EUCAP)*, Rome, pp. 3905–3908 (2011).
- B. Wang, W. Yezunian, and K. H. Teo, "Wireless power transfer: metamaterials and array of coupled resonators," *Proc. IEEE* **101**(6), 1359–1368 (2013).

Cumali Sabah received his BSc, MSc, and PhD degrees in electrical and electronics engineering. Currently, he is an associate professor in the Electrical and Electronics Engineering Department at Middle East Technical University—Northern Cyprus Campus, where he is secretary general and advisor to the president. His research interests include the microwave and electromagnetic investigation of unconventional materials and structures, wave propagation, scattering, complex media, MTMs and their applications, and solar systems.

Biographies for the other authors are not available.